Mechanics & Industry **19**, 603 (2018)
© AFM, EDP Sciences 2019
https://doi.org/10.1051/meca/2018045

Mechanics & Industry

Available online at:
www.mechanics-industry.org

Regular Article

Comparison between conventional shot peening and ultrasonic shot peening

Sondes Manchoul[1], Rabi Ben Sghaier[1,2,*], Rawdha Seddik[1], and Raouf Fathallah[1]

[1] Université de Sousse, National Engineering School of Sousse, BP 264, Erriadh, 4023 Sousse, Tunisia
[2] Université de Sousse, Institute of Applied Sciences and Technology of Sousse, Cité Taffala (Ibn Khaldoun), 4003 Sousse, Tunisia

Received: 24 September 2017 / Accepted: 20 November 2018

Abstract. Shot peening process is a mechanical surface treatment process widely used in the industry. Ultrasonic shot peening and conventional shot peening are two important mechanisms of this process. This work aims at studying and comparing the influence of conventional shot peening and ultrasonic shot peening on the surface characteristics (residual stresses, equivalent plastic deformations, and roughness). Three-dimensional models are established to simulate the two mechanisms by using the finite elements software ABAQUS/PYTHON. The residual stresses distributions, as well as the roughness and the equivalent plastic deformations of the AISI 2205 and the AISI 316L induced by both models, are predicted and compared.

Keywords: Ultrasonic shot peening / conventional shot peening / residual stresses / roughness / finite elements

1 Introduction

Conventional shot peening (CSP) is one of the popular surface enhancement processes. It consists of projecting small shots at the surfaces of the metallic components. Ultrasonic shot peening (USP) is based on the same principle as CSP. The differences between both mechanisms were highlighted by Todaka et al. [1]: the size of shot (between 0.25 and 1 mm for CSP, and 1 and 8 mm for USP) and the velocity (between 20 and 150 m/s for CSP, and 3 and 20 m/s for USP). Another difference is the mechanism used for projecting the shots. In USP process the shots, confined in a closed chamber, are projected by sonotrode vibration on the treated specimen that is fixed on the top of this chamber. Thus, during the USP, the shots can be recovered after the treatment. These differences have a significant impact on surface characteristics and mechanical properties. Hence, predicting the influence of both processes on surface characteristics and providing a quantitative description of all these differences present a scientific interest.

Many finite element (FE) simulations were performed to predict principally the residual stress fields induced by the CSP process. Frija et al. [2] presented a three-dimensional FE model allowing to predict the compressive residual stresses (CRS) fields, the plastic strain, and particularly the superficial damage. This model has the advantage of predicting the majority of the initial effects induced by shot peening. Whereas it didn't consider the effect of the cyclic elastic-plastic hardening, Taehyung et al. [3] developed a three-dimensional model of CSP, which leads to predict the CRS fields resulting from numerous impacts. There were other numerical models that simulated the CSP; only a few ones are available regarding USP process. Indeed, because of the complexity of the USP mechanism, its numerical simulation is rarely reported. Chaise et al. [4] gave a specific USP model to compute residual stress after normal impacts. Rousseau et al. [5] examined the effect of shots number in an ultrasonic-peened target, showing that an increase in the bead quantity significantly concentrates the CRS into the treated components. In this present paper, we propose two realistic models that can quantify the differences in the residual stress state as well as in the roughness for the USP and CSP mechanisms.

2 Finite element modelling

The USP and CSP simulations are carried out by the use of finite element code ABAQUS 6.10 [6]. A numerical code is developed on the basis of Python script to automatically generate, with particular parameters (diameter, velocity, and the number of shots...) each process. The two models are composed of elastic-plastic shots that impact a semiinfinite structure. An explicit surface-to-surface contact with friction is defined between the surfaces of the target and the spherical shots. A kinematic contact algorithm is selected to model the shot-target interactions [6].

* e-mail: rabibensghaier@gmail.com

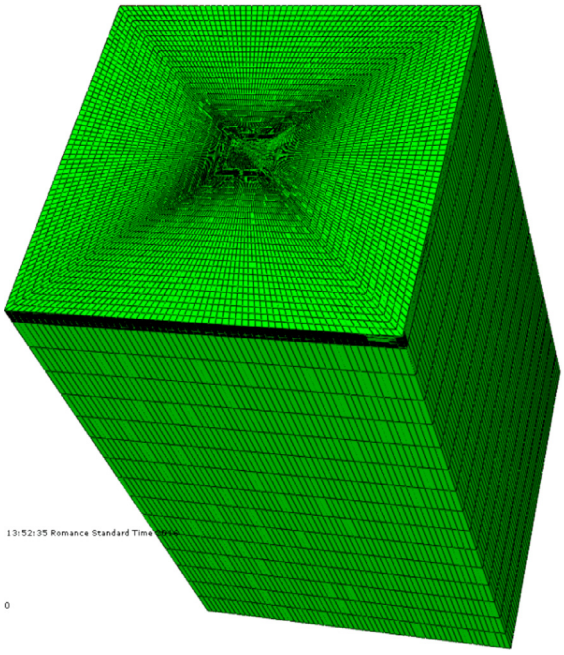

Fig. 1. Impacted mass if used in the two models.

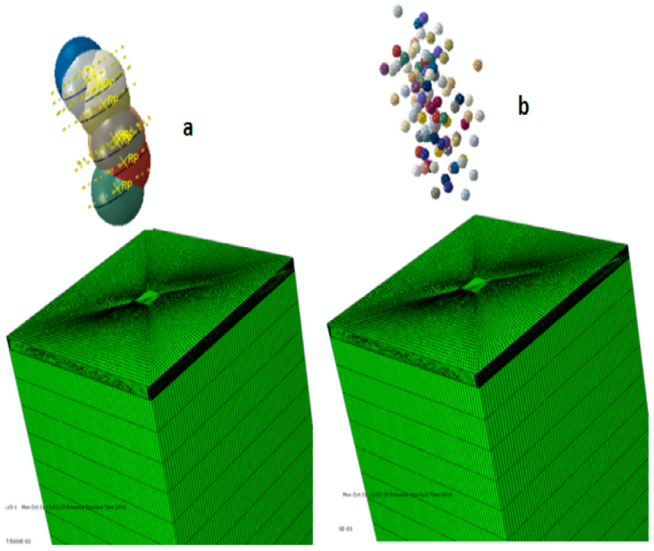

Fig. 2. (a) USP model. (b) CSP model.

2.1 Target geometry and boundary conditions

The target component (Fig. 1) used in the two models is represented by a rectangular body. Eight-node linear brick solid elements with reduced integration are utilized to mesh it [6]. The width, length, and height of the target are set at 20, 20, and 35 mm. The target includes two regions in the X–Y plane as shown in Figure 1. The region located at the center of the target is reduced to 2 mm width, 2 mm length, and 1 mm height. The central area is the local of the shots' impacts. To improve the accuracy of the FE solutions, this region is finely meshed. For the boundary condition, the bottom surface of the target is fixed and restrained against all displacements. Shots are modeled as deformable spherical bodies meshed with C3D4 four-node linear tetrahedron elements [6].

2.2 Ultrasonic shot peening model

The impact velocity is a critical parameter for the USP model. Chaise et al. [4] reported that the average impact velocity could be as large as the impact maximal velocity of the ultrasonic transducer. Hence, the USP simulation considers all the impacts at a constant and maximal velocity, which is expressed as follows [4]:

$$V_{\max} = A2\pi F, \tag{1}$$

where A is the amplitude of vibration of the sonotrode, and F is the frequency of vibration. The frequency of vibration considered in this work is 20 kHz.

The USP model (Fig. 2a) involves a small number of spherical shots, with a big diameter, impacting the surface at low velocity. It has been inferred that all shots impact the target with an impact angle close to 90° as the collisions between shots are neglected in this work [4].

2.3 Conventional shot peening model

For the CSP model (Fig. 2b), we utilize many shots with small diameter hitting the surface (central region) randomly with an angle of impingement equal to 90°. Shots in CSP model involve a high impact velocity.

It should be noted that all the peening parametres (diameter, velocity, etc.) used in both models are chosen, adequately, in order to approach to the real situation of the two processes (CSP and USP).

2.4 Isotropic–kinematic constitutive model

The convenient shot peening behavior law of the treated material has to reflect the effect of the cyclic loading [7]. In this study, the nonlinear isotropic–kinematic hardening [8] law is used to model both the CSP and the USP process. The yield criterion of Von Mises is defined as follows:

$$f(\overline{\overline{\sigma}}, \overline{\overline{X}}, R) = J_2(\overline{\overline{\sigma}} - \overline{\overline{X}}) - R - K \leq 0. \tag{2}$$

The nonlinear hardening component is defined as

$$d\overline{\overline{X}} = \frac{2}{3} C d\overline{\overline{\varepsilon^p}} - \gamma \overline{\overline{X}} dp. \tag{3}$$

The isotropic hardening component R describes the change of the equivalent stress, which defines the size of the yield surface as a function of plastic deformation:

$$dR = b(Q - R)dp, \tag{4}$$

where

$$dp = \sqrt{\frac{2}{3} d\overline{\overline{\varepsilon^p}} : d\overline{\overline{\varepsilon^p}}}, \tag{5}$$

Table 1. Mechanical properties of AISI 316L [9] and AISI 2205 [10].

Material	AISI 2205	AISI 316L
E (GPa)	192.5	196
σ_y (MPa)	632	220
υ	0.3	0.29
C (MPa)	192.777	30
γ	575	60
Q (MPa)	−23	150
b	13	1

Table 2. The experimental peening conditions.

Peening conditions	Shots materials	V (m/s)	D (mm)	Angle (°)
Ahmed [13]	ceramic	40	0.8	90
Sanjurjo [10]	Steel	40	0.6	90
Li [14]	100Cr6 steel	4	4	90

where dp indicates the increment of the equivalent plastic strain, $\mathrm{d}\overline{\overline{\varepsilon^p}}$ is the plastic flow law, which is defined as

$$\mathrm{d}\overline{\overline{\varepsilon^p}} = \lambda \frac{\delta f}{\delta \overline{\overline{\sigma}}}. \tag{6}$$

The coefficients depending on the material are Q and b the parameters of the isotropic hardening, C and γ the two coefficients that represent the evolution of the kinematic hardening, and σ_y is the initial yield stress. The mechanical properties of the two studied materials AISI 316L and AISI 2205 are presented, respectively, in the Table 1 [9,10]. As mentioned in this table, the yield strength of AISI 316 L is equal to 220 MPa [9] and the yield strength of AISI 2205 is equal to 623 MPa [10].

In the majority of the modellling work, the shots are supposed to be rigid. In the present work, it is assumed that the steel shots have an elastoplastic [3] behavior and those on ceramic have an elastic behavior [3] in order to take into account the effect of the part of the kinetic energy absorbed by the shots [3,11,12].

3 The proposed criterion to compare the two processes

To compare the CSP and USP, we consider the same kinetic energy (E_K) and the same coverage in both models.

3.1 Kinetic energy

The kinetic energy of the shots in shot peening process is given by

$$E_K(SP) = \frac{\pi}{12}\rho D^3 V^2 N, \tag{7}$$

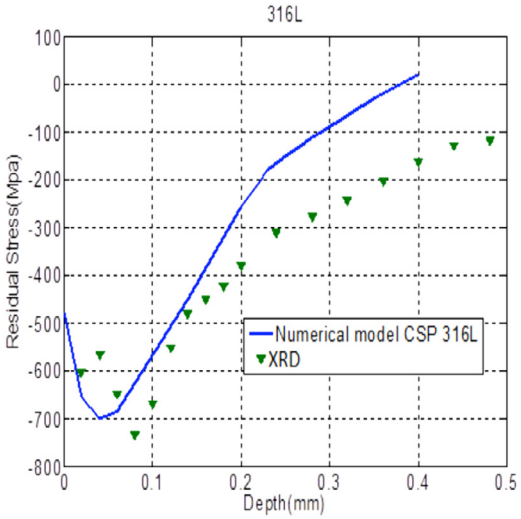

Fig. 3. Validation of CSP model for AISI 316l [13].

where N is the number of shots hiding the target, D is the diameter of the shots, and V is the impact velocity.

3.2 Peening coverage

The peening coverage presents a crucial peening parameter since it has an influence on the CRS profile. It is defined as the percentage of the surface that is impacted for a given time of peening. The full coverage (100%) is reached when the treated surface is entirely impacted. To determine the impacted surface, it is necessary to predict the radius of shots indentation, which is expressed as follows [7]:

$$a = \frac{D}{2}\left(\frac{5prK(1-e_r)n^2}{2E^*}\right)^{1/5}, \tag{8}$$

where a is the radius of indentation for a shot impact, D is the diameter of shots, v is the shot velocity, ρ is the density of shots, e_r is the coefficient of restitution, E^* is the equivalent stiffness modulus, and k is the efficiency coefficient.

4 Application

4.1 Validation of the CSP and the USP models

In order to validate the accuracy of the proposed CSP model, the peening conditions used by Ahmed's experimental investigations [13] for the AISI 316L material are considered in this study. The experimental peening conditions, extracted from the literature, used to validate the numerical models are summarized in Table 2.

Figure 3 shows a good correlation between the experimental investigation [13] and the computed results. It can be noted that for large depths, there is a disagreement between the predicted CSP model and the experimental results. Here, it is important to note that both numerical and experimental profiles induced by shot peening should show a state of equilibrium between tensile and

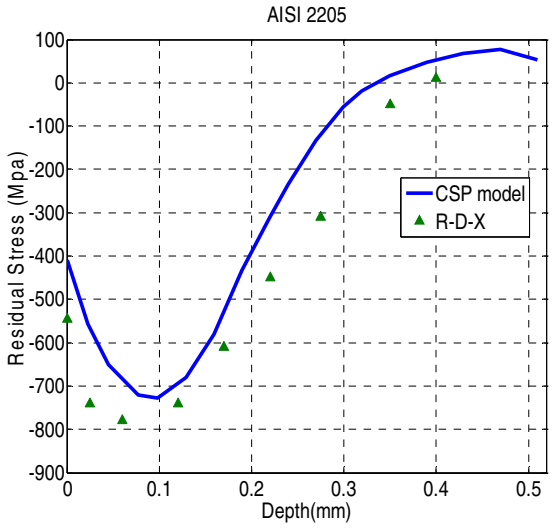

Fig. 4. Validation of CSP model for AISI 2205 [10].

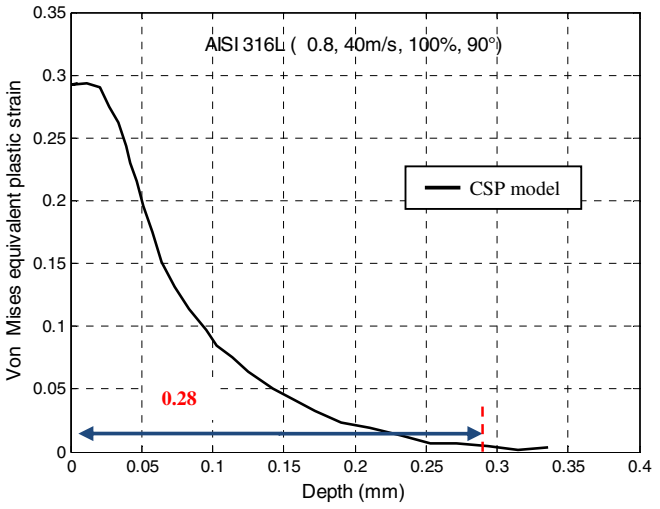

Fig. 6. Distribution of plastic equivalent strain (PEEQ) after conventional shot peening for AIS 316L target.

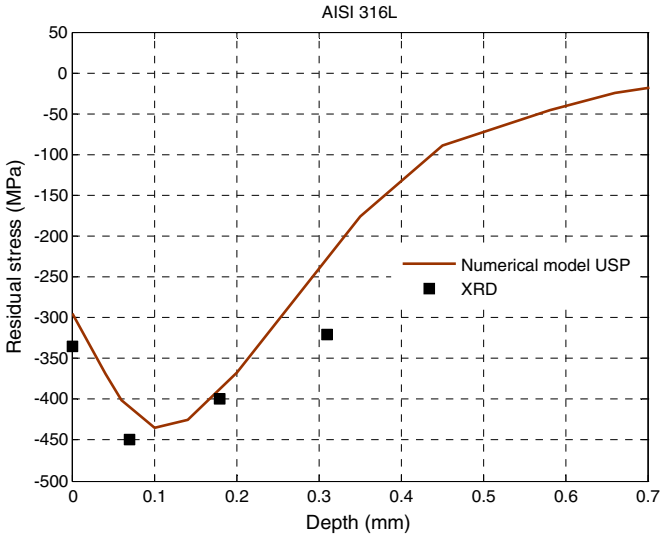

Fig. 5. Validation of USP model for AISI 316L [14].

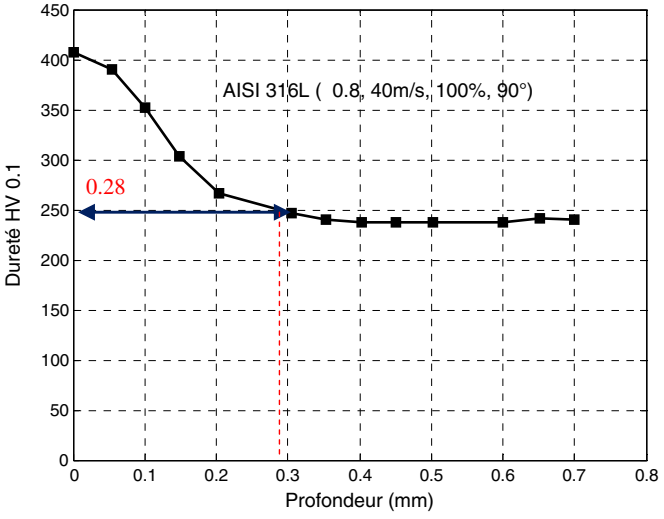

Fig. 7. Microhardness–depth distribution after conventional shot peening for AIS 316L.

compressive residual stresses. In Figure 3, the in-depth RS profile induced by FE model matched better with the physical phenomenon of equilibrium than the diffraction measurements that support the reliability and the validity of the presented numerical simulation. Hence, the reason for this gap may originate from the uncertainties of the X-ray diffraction analysis, especially in the etched depths. In fact, the profiles of residual stresses obtained by X-ray measurements are generally more precise in the first outer layers than in the deeper ones, owing to difficulties to obtain perfectly planed surfaces by electrochemical polishing in terms of deeper layers.

For the AISI 2205, we consider the same conventional peening conditions used by Sanjurjo [10] in his experimental results. A good agreement between the computed values and the experimental results [10] is obtained as shown in Figure 4.

For the AISI 316 L, the operating conditions used by Li in his experimental investigations [14] are considered in this numerical application so as to verify the accuracy of the established USP model.

Figure 5 indicates a good coordination for predicting the initial CRS profiles for the AISI 316L material comparing with the experimental results obtained by the X-ray diffraction analysis [14].

Figure 6 depicts the profile of the plastic strain as a fuction of the position that is determined from the contact point after CSP impact. The profile shows that the maximum of the equivalent plastic strain is at surface and there is a short plateau near the sample surface.

Figures 6 and 7 present a qualitative comparison between the profiles of the Von Mises equivalent plastic deformations obtained by simulation and the experimental [13] hardness distributions across the treated target.

Table 3. The input data used in the numerical models.

Models	V (m/s)	N	D (mm)	EK (J)
USP	4	10	4	0.0208
CSP	40	100	0.4	0.0208

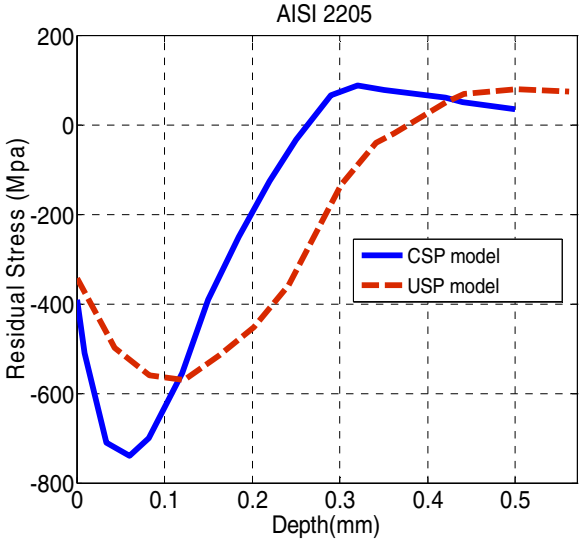

Fig. 8. Residual stresses induced in the AISI 2205 target by CSP and USP.

Figure 6 indicates that the deformed layer induced by CSP model is 0.28 mm. The qualitative comparison between the numerical profile of Von Mises equivalent plastic deformations (Fig. 6) and the experimental distribution of microhardness [13] (Fig. 7) shows that the shot peening deformed layer is well predicted.

4.2 Application of the proposed criterion of comparison

Table 3 summaries all the input data related to the shot sizes, the velocities of impacts considered in the CSP and USP simulations. In this study, the amplitude A of the vibration used is $A = 32\,\mu$m. As a result, the impact velocity used in the USP is 4 m/s.

It can be seen from Table 3 that the differences between the USP and the CSP lie in the impact velocities, the size, and the number of used shots. To better describe the real situation of the two processes, the size of shots in the USP model is supposed to be 10 times higher than the CSP ones, while the impact velocity is 10 times smaller. This discrepancy in the diameter and velocity range causes, in turn, a decrease in the provided energy of impact acquired by shots for the CSP process. Such differences have a significant effect on the surface characteristics and the mechanical properties [15]. Consequently, to compensate for the low energy caused by the lower size and to have hypothetically the same E_K, a large number of shots are utilized (100 shots) in the CSP model, while only 10 shots

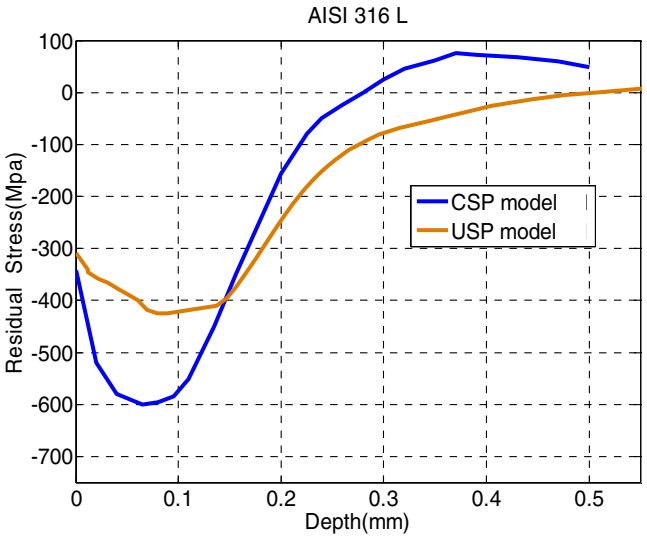

Fig. 9. Residual stresses induced in the AISI 316L target by CSP and USP.

are considered in the USP model. In this study, we propose two FE models to provide a quantitative description of these differences between the CSP and USP treatments. The implementation of these simulations allows examining the exact effect of the shot velocity and size on the surface conditions induced by both processes when having an identical kinetic energy.

Considering the previous hypotheses and referring to equation (8), the evaluated radius of indentation for a USP shot impact is about three times higher than the one resulted from the CSP. As the surface of indentation induced by one shot impact is $2\,\pi\,a^2$, 10 shots are required in the CSP simulation to achieve the same surface of impact obtained by one shot in the USP. Hence, the 100 shots utilized in the CSP model allow having the same coverage realized by 10 shots in the USP one.

5 Results and discussion

5.1 Comparison of residual stress state

Figures 8 and 9 provide a comparison between the profiles of residual stress induced by the CSP and USP performed, respectively, on the AISI 2205 and AISI 316 L materials. The two figures show that for both materials

- at the surfaces, the resulting CRS at the surfaces for USP and CSP processes are comparable;
- the subsurface CRS maximum in the conventional peened target is higher than for ultrasonic peened one;
- the thickness of compressive residual stress is deeper for USP treatment than the CSP one.

The numerical results suggest that for an equal E_K and coverage between the CSP and USP processes, small shots with higher velocity result in a higher CRS maximum than bigger shots, whereas bigger shots used in USP produce a deeper residual stress layer. These differences between the USP and CSP processes could have a

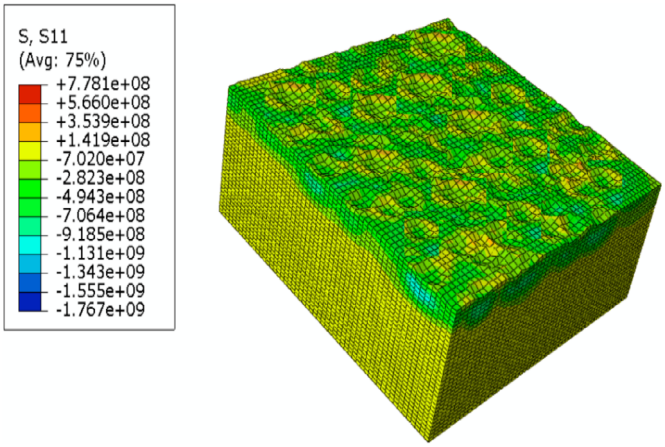

Fig. 10. Distribution of residual stress induced by CSP model for AISI 316L.

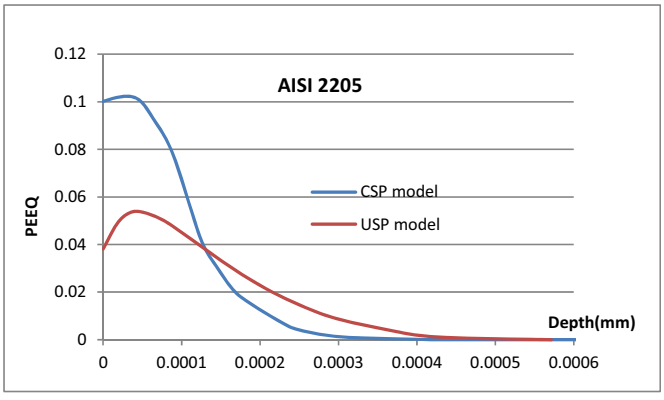

Fig. 11. Distribution of equivalent strain plastic (PEEQ) after ultrasonic shot peening for AIS 2205 target.

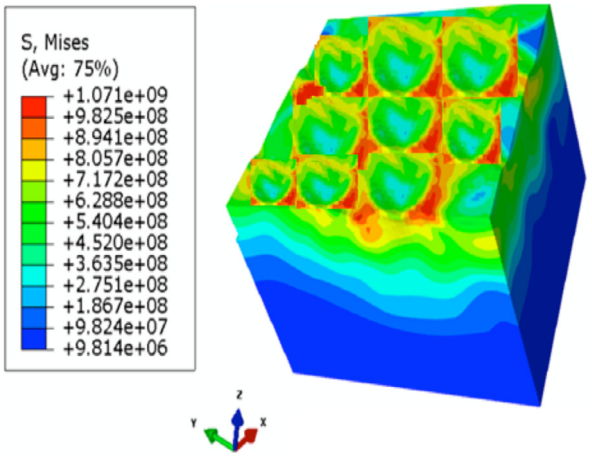

Fig. 12. The equivalent plastic stress induced by USP for AISI 2205 material.

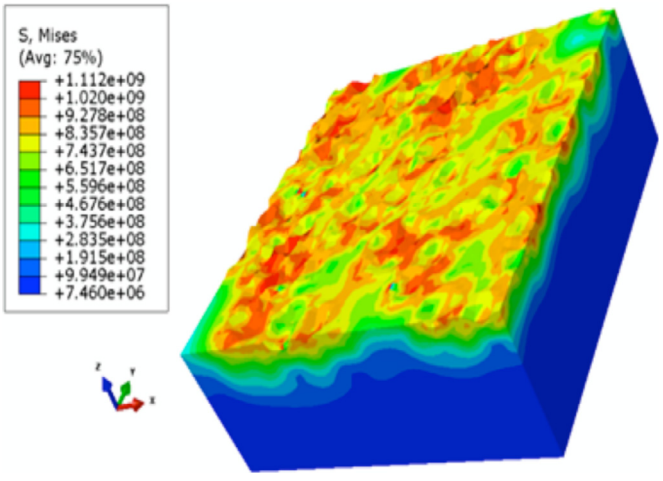

Fig. 13. The equivalent plastic stress induced by CSP for AISI 2205 material.

significant effect on the fatigue surface characteristics of the peened part.

Figure 10 shows the distribution of residual stress for the AISI 316L peened target after the CSP simulation. Note that multiple impacts of 100 impacts were run to obtain approximately a compressive residual stress field at the surface.

Additionally, Figure 11 reveals that the depth of the plastic zone in the case of USP is about 0.6 mm, which is substantially deeper than the one resulted from CSP model. Moreover, the FE results suggest that for an identique E_k between the CSP and USP processes, shots with smaller size and higher velocity result in a higher maximum of PEEQ than bigger shots.

The equivalent plastic stress induced by the USP and CSP processes, having the same coverage percentage (100%) and the same E_K upon the AISI 2205, are given, respectively, in Figures 12 and 13.

5.2 Roughness and geometrical stress concentration factor

Shot peening surface treatment is generally aimed at enhancing the resistance of metallic mechanical components. However, in some cases, there is a risk of changing the integrity of the treated surface by inducing superficial defects such as micro cracks, scales, overlaps, and surface roughness imperfections, which can induce a significant decrease of fatigue strength. Indeed, the surface roughness can provoke stress concentration at specific points and also facilitates crack initiation.

In the present work, the two proposed finite elements models have been applied to predict the critical surface roughness parameters: (i) R_{tm}, which is defined as the average of the lowest and highest point between dents and (ii) S_{m}, which is the distance between adjacent peaks (Fig. 14).

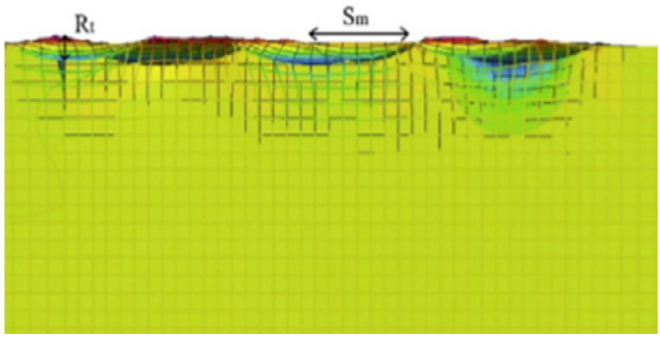

Fig. 14. The equivalent plastic stress induced by CSP for AISI 2205 material.

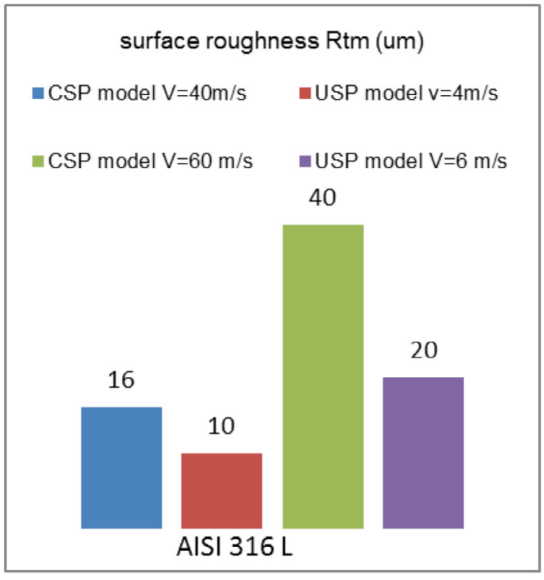

Fig. 15. Comparison between the computed roughness (R_{tm}) for CSP and USP models.

Based on the study of Mylonas [16], the geometrical stress concentration factor (K_t) has been also calculated using the computed roughness parameters mentioned earlier. This factor K_t indicates the critical peened zone from which a crack may initiate. Indeed, it is approximated by the following expressions [16]:

$$K_t = 1 + 4\left(\frac{R_{\mathrm{tm}}}{S_m}\right)^{1.3} \left(\frac{R_{\mathrm{tm}}}{S_m} \prec 0.15\right), \tag{9}$$

$$K_t = 1 + 2.1\left(\frac{R_{\mathrm{tm}}}{S_m}\right) \left(\frac{R_{\mathrm{tm}}}{S_m} \leq 0.3\right). \tag{10}$$

Figure 15 shows a comparison between numerically computed surface roughness R_{tm} for CSP and USP models. As can be seen, the CSP results in a rougher surface ($R_{\mathrm{tm}} = 16\,\mu\mathrm{m}$) than the USP one ($R_{\mathrm{tm}} = 10\,\mu\mathrm{m}$). Thus, this figure proves the experimental results that show an important difference between CSP and USP concerning the roughness. This higher roughness induced by CSP is caused by the very high velocity of impact attributed to shots [17]. Besides, it shows that for each model, the rising velocity (i.e., from 4 to 6 m/s for USP model) leads to an increase in surface roughness (from 10 to 20 µm, respectively).

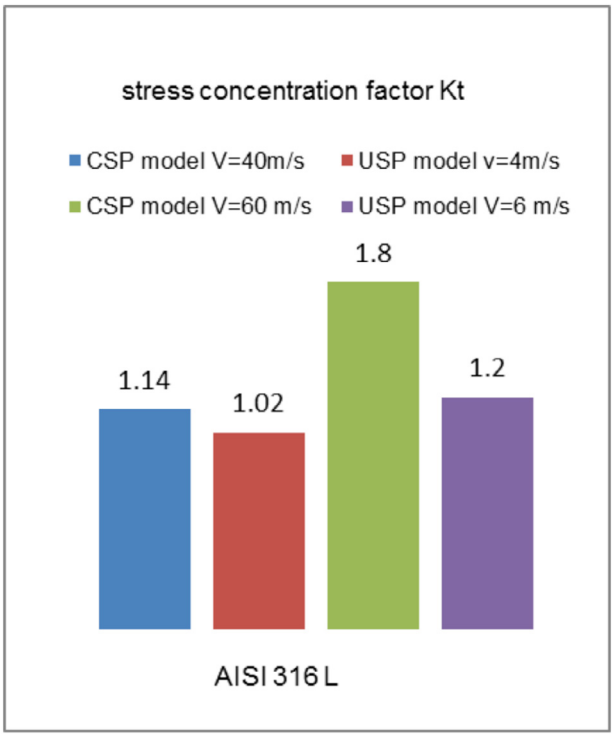

Fig. 16. Comparison between the computed (K_t) for USP and CSP models.

Figure 16 illustrates that CSP process increases the geometrical stress concentration factor K_t more than the USP one (especially for high velocities).

6 Conclusion

This paper presents 3D finite element models able to point out at the differences in the CRS between USP and CSP mechanisms: USP induces deeper residual stress layer, while the CSP results on higher subsurface CRS maximum. Moreover, the proposed models allow predicting the geometric stress concentration factor using the computed results as imputed data to analytical equations. This present study approved, numerically, that main benefit of USP compared to CSP is the low roughness of the surface, which is due to the lower impact velocities. It remains now to adopt a fatigue criterion that takes into account these CRS to determine which process further improves fatigue resistance.

Nomenclature

A	Amplitude of vibration of the sonotrode
C, γ	Material constants of the nonlinear kinematic hardening law
b, Q	Material constants of the isotropic hardening law

E, E^*	Elastic and equivalent stiffness modulus, respectively
υ	Poisson's ratio
ρ	Density
V	Shot velocity
k, e_r	Efficiency and restitution coefficients, respectively
σ_y	Yield strength
E_K	Kinetic energy of the shots
f	Yield surface defined by the Von Mises criterion
F	Frequency of vibration
R	Frequency variable of the isotropic law
R_{tm}	Average of the highest and lowest point between dents
S_{m}	Distance between adjacent peaks.
N	Number of shots
K_t	Geometrical stress concentration factor
dp	Increment of the equivalent plastic strain
λ	Wave length of the X-ray
$\underline{X}$	Variable of the nonlinear kinematic hardening law
$\underline{\underline{\sigma}}$, $\underline{\underline{\varepsilon^p}}$	Stress and plastic strain tensors, respectively

References

[1] Y. Todaka, M. Umemoto, K. Tsuchiya, Comparison of nanocrystalline surface layer in steels formed by air blast and ultrasonic shot peening, Mater. Trans. 45 (2004) 376–379

[2] M. Frija, T. Hassine, R. Fathallah, C. Bouraoui, A. Dogui, FEM modelling of shot peening process: prediction of the compressive residual stresses, the plastic deformations and the surface integrity, Mater. Sci. Eng. 426 (2006) 173–180

[3] K. Taehyung, L. Hyungyil, K. Minsoo, J. Sunghwan, A 3D FE model with plastic shot for evaluation of equi-biaxial peening residual stress due to multi-impacts, Surf. Coat. Technol. 206 (2012) 3981–3988

[4] T. Chaise, J. Li, D. Nelias, R. Kubler, S. Taheri, G. Douchet, V. Robin, P. Gilles, Modelling of multiple impacts for the prediction of distortions and residual stresses induced by ultrasonic shot peening (USP), J. Mater. Process. Technol. 212 (2012) 2080–2090

[5] T. Rousseau, T. Hoc, P. Gilles, C. Nouguier-Lehon, Effect of bead quantity in ultrasonic shot peening: surface analysis and numerical simulations, J. Mater. Process. Technol. 225 (2015) 413–420

[6] ABAQUS Theory Manual, Version 6.10, Hibbitt, Karlsson and Sorensen Inc., USA, 2011

[7] R. Fathallah, Modélisation du Procédé de Grenaillage: Incidence des Billes et Taux de Recouvrement, PhD thesis, ENSAM, Paris, 1994

[8] J.-L. Chaboche, Sur l'utilisation des variables d'état interne pour la description de la viscoplasticité cyclique avec endommagement, in Problèmes Non Linéaires de Mécanique, Symposium Franco-Polonais de Rhéologie et Mécanique, 1977, pp. 137–159

[9] A. Laamouri, H. Sidhom, C. Braham, Evaluation of residual stress relaxation and its effect on fatigue strength of AISI 316Lstainless steel ground surfaces: experimental and numerical approaches, Int. J. Fatigue 48 (2013) 109–121

[10] P. Sanjurjo, C. Rodríguez, I. Peñuelas, T.E. García, F. Javier Belzunce, Influence of the target material constitutive model on the numerical simulation of a shot peening process, Surf. Coat. Technol. 258 (2014) 822–831

[11] R. Seddik, A. Bahloul, A. Atig, R. Fathallah, A simple methodology to optimize shot-peening process parameters using finite element simulations, Int. J. Adv. Manuf. Technol. 90 (2017) 2345–2361

[12] R. Seddik, R. Ben Sghaier, R. Fathallah, A numerical-analytical approach to predict the effects of shot peening on the fatigue performance of the nickel-based super alloy Waspaloy, Proc. Inst. Mech. Eng. Part L: J. Mater. Des. Appl. (2016). DOI: 10.1177/1464420716663030

[13] A.A. Ahmed, M. Mhaede, M. Basha, M. Wollmann, L. Wagner, The effect of shot peening parameters and hydroxyapatite coating on surface properties and corrosion behavior of medical grade AISI 316L stainless steel, Surf. Coat. Technol. 280 (2015) 347–358

[14] J. Li, Simulation de Réparation par Soudage et Billage Ultrasonore d'un Alliage à base nickel, PhD thesis, LaMCoS, Lyon, 2011

[15] K. Dai, L. Shaw, Comparison between shot peening and surface nanocrystallization and hardening processes, Mater. Sci. Eng. A. 463 (2007) 46–53

[16] G.I. Mylonas, G. Labeas, Numerical modelling of shot peening process and corresponding products: residual stress, surface roughness and cold work prediction, Surf. Coat. Technol. 205 (2011) 4480–4494

[17] R. Ben Sghaier, Ch. Bouraoui, R. Fathallah, G. Degallaix, High cycle fatigue based reliability design of welded and shot peened high strength steel, Fatigue Fract. Eng. Mater. Struct. 33 (2010) 575–594

Cite this article as: S. Manchoul, R. Ben Sghaier, R. Seddik, R. Fathallah, Comparison between conventional shot peening and ultrasonic shot peening, Mechanics & Industry **19**, 603 (2018)